V26 : 24 July 2018

Photoionization dynamics of cis-dichloroethene from investigation of vibrationally resolved photoelectron spectra and angular distributions

I. Powis,[a*] R. C. Menzies,[a] D. M. P. Holland,[b] A. B. Trofimov,[c,d] A. D. Skitnevskaya,[c] E. V. Gromov,[e] E. Antonsson,[f,g] M. Patanen,[f,h] C. Nicolas,[f] and C. Miron[f,i]

[a] School of Chemistry, University of Nottingham, Nottingham NG7 2RD, United Kingdom

[b] Daresbury Laboratory, Daresbury, Warrington, Cheshire WA4 4AD, United Kingdom

[c] Laboratory of Quantum Chemistry, Irkutsk State University, Karl Marx Str. 1, 664003 Irkutsk, Russia

[d] Favorsky's Institute of Chemistry, SB RAS, Favorsky Str. 1, 664033 Irkutsk, Russia

[e] Theoretische Chemie, Physikalisch-Chemisches Institut, Universität Heidelberg, Im Neuenheimer Feld 229, 69120 Heidelberg, Germany

[f] Synchrotron SOLEIL, l'Orme des Merisiers, Saint-Aubin, BP 48, 91192 Gif-sur-Yvette, France

[g] *Current Address*: Physical Chemistry, Freie Universität Berlin, Takustr. 3, D-14195 Berlin, Germany

[h] *Current Address*: Nano and Molecular Systems Research Unit, Faculty of Science, P. O. Box 3000, 90014 University of Oulu, Finland

[i] *Current Address*: LIDYL, CEA, CNRS, Université Paris-Saclay, CEA Saclay, 91191 Gif-sur-Yvette, France

*Corresponding Author

Email: ivan.powis@nottingham.ac.uk

Tel: +44 115 9513467

ABSTRACT

The influence of vibronic coupling on the outer valence ionic states of cis-dichloroethene has been investigated by recording photoelectron spectra over the excitation range 19 – 90 eV using plane polarized synchrotron radiation, for two polarization orientations. The photoelectron anisotropy parameters and electronic state branching ratios derived from these spectra have been compared to theoretical predictions obtained with the continuum multiple scattering approach. This comparison shows that the photoionization dynamics of the $\tilde{A}\ ^2B_2$, $\tilde{B}\ ^2A_1$, $\tilde{C}\ ^2A_2$ and $\tilde{D}\ ^2B_1$ states, all of which are formed through the ejection of an electron from a nominally chlorine lone-pair orbital, exhibit distinct evidence of the Cooper minimum associated with the halogen atom. While retaining a high degree of atomic character these orbital ionizations nevertheless display clear distinctions. Simulations, assuming the validity of the Born-Oppenheimer and the Franck-Condon approximations, of the $\tilde{X}\ ^2B_1$, $\tilde{A}\ ^2B_2$ and $\tilde{D}\ ^2B_1$ state photoelectron bands have allowed some of the vibrational structure observed in the experimental spectra to be assigned. The simulations provide a very satisfactory interpretation for the $\tilde{X}\ ^2B_1$ state band but appear less successful for the $\tilde{A}\ ^2B_2$ and $\tilde{D}\ ^2B_1$ states, with irregularities appearing in both. The $\tilde{B}\ ^2A_1$ and $\tilde{C}\ ^2A_2$ state photoelectron bands exhibit very diffuse and erratic profiles that cannot be reproduced at this level. Photoelectron anisotropy parameters, β, have been evaluated as a function of binding energy across the studied photon energy range. There is a clear step change in the β values of the $\tilde{A}\ ^2B_2$ band at the onset of the perturbed peak intensities, with β evidently adopting the value of the $\tilde{B}\ ^2A_1$ band β. The $\tilde{D}\ ^2B_1$ band β values also display an unexpected vibrational level dependence, contradicting Franck-Condon expectations. These various behaviours are inferred to be a consequence of vibronic coupling in this system.

I. INTRODUCTION

The three isomers (cis, trans and iso) of dichloroethene ($C_2H_2Cl_2$) provide an ideal means of studying substitution effects on the valence shell electronic structure and photoionization dynamics. The present study concerns cis-1,2-dichloroethene and reveals that vibronic interactions between neighbouring ionic states[1,2] not only influence photoelectron band envelopes and the associated vibrational structure but also the photoelectron angular distributions.

The photoelectron spectrum of the unsubstituted parent molecule (ethene, C_2H_4) was one of the first in which the influence of vibronic interactions on the electronic structure was studied in detail.[3,4] A good summary of our current understanding of these effects on the ionic states of ethene has been given by Hazra and Nooijen.[5,6] The theoretical work shows that, although vibronic coupling occurs between the ground ionic state and the first excited ionic state, non-adiabatic effects in the ionic ground state are weak. The calculated $\tilde{X}$ state photoelectron spectrum[5] reproduced the vibrational structure observed experimentally.[7] In contrast, the experimental photoelectron spectra for the $\tilde{A}$, $\tilde{B}$ and $\tilde{C}$ states of ethene are difficult to interpret, exhibiting only a few broad peaks.[7] These diffuse photoelectron bands, which are simulated satisfactorily in the vibronic coupling calculations,[6] are the result of significant non-adiabatic effects in all three excited ionic states.

It is now well established that vibronic interactions between ionic states can radically alter the vibrational structure in a photoelectron band from that expected from models employing the Born-Oppenheimer and Franck-Condon approximations.[1] Such models are based upon the concept that each electronic state has an associated isolated potential energy surface. Vibronic coupling, namely the interaction of two or more energetically close-lying electronic states

through the nuclear motion, results in a breakdown of the Born-Oppenheimer approximation. The ensuing non-adiabatic effects, which account for motion of the nuclei on more than one potential energy surface, can lead to changes in the vibrational structure. These can vary between slightly irregular vibrational energy spacings and/or peak intensities — but still recognisable vibrational progressions — in the case of weak vibronic coupling, to a complete loss of any distinguishable vibrational pattern for strong vibronic coupling. In the latter case, vibronic coupling calculations predict numerous vibrational excitations, some of which involve non-totally symmetric vibrational modes. The summation of these excitations can result in a diffuse photoelectron band.

Vibronic coupling has also been predicted to affect the photoionization dynamics[8,9] as characterized by the photoelectron anisotropy parameter (β). Boron trifluoride provides a good example of such behaviour.[10] Franck-Condon forbidden excitation of a single quantum of the non-totally symmetric $\nu_3^+(e')$ mode in the $\tilde{E}\ ^2A_1'$ state photoionization can be ascribed to vibronic coupling between the $\tilde{D}\ ^2E'$ and the $\tilde{E}\ ^2A_1'$ ionic states. The anisotropy parameters for these perturbed $\tilde{E}\ ^2A_1'$ state excitations were similar to those of the $\tilde{D}\ ^2E'$ state and differed considerably from those of unperturbed $\tilde{E}\ ^2A_1'$ excitations. Thus, the experimental results confirmed the predictions by Haller et al.[8] that the anisotropy parameters associated with photoelectron peaks induced by vibronic coupling should reflect those of the state to which they are coupling, and from which they derive their intensity.

In this paper we present experimental results, including photoelectron spectra, electronic branching ratios and anisotropy parameters, obtained for cis-dichloroethene. Vibrational structure is analysed at the Franck-Condon level of approximation with the help of simulations of the vibrational envelope, and the photoionization dynamics are likewise modelled using electron multiple

scattering calculations.[11] In a companion paper[12] we give a more complete theoretical treatment of the vibronic interactions coupling the $\tilde{A}\ ^2B_2$, $\tilde{B}\ ^2A_1$ and $\tilde{C}\ ^2A_2$ states, and the $\widetilde{D}\ ^2B_1$ and $\tilde{E}\ ^2B_2$ states that can be inferred from the present results and analysis. Consideration of the inner valence region is also deferred to that paper.

The outer valence shell orbital sequence of cis-dichloroethene in its molecular ground state may be written as (using C_{2v} symmetry)

$(9a_1)^2(8b_2)^2(2b_1)^2(2a_2)^2(10a_1)^2(9b_2)^2(3b_1)^2$.

Mulliken atomic populations[13] allowing the character of these molecular orbitals to be assessed are reproduced in Table I and visual representations of these orbitals are given in Figure 1. The outermost $3b_1$ orbital has a mixed carbon and chlorine character but the next four lower occupied orbitals ($9b_2$, $10a_1$, $2a_2$ and $2b_1$) contain a significant Cl 3p content. These four orbitals comprise essentially two in-plane and two out-of-plane chlorine lone-pairs, and for brevity we will henceforth use σ or π to identify, respectively, the in-plane or out-of-plane orientation of the halogen '*p*' orbitals. Photoelectron bands associated with nominally lone-pair orbitals are usually dominated by an intense adiabatic transition and have little accompanying vibrational structure.[14] However, our experimental and simulated spectra show that this is not the case for these orbitals ($9b_2$, $10a_1$, $2a_2$ and $2b_1$) in cis-dichloroethene.

The high Cl 3p content in the lone-pairs will manifest itself in the photoelectron angular distributions and the photoionization partial cross sections associated with these molecular orbitals. Specifically, the Cooper minimum[15,16] associated with a Cl 3p orbital[17] will, in the atomic limit, result in a fairly isotropic photoelectron angular distribution and a reduction in the partial cross section in the photon energy range around 40 eV. Such effects have also been observed

previously in chlorine containing molecules[18-21] and can be used to assess the extent to which the atomic orbital is modified by the molecular environment.

Previous experimental investigations on cis-dichloroethene include photoelectron spectra recorded with HeI [22-26] HeII,[26] Al Kα,[27] and synchrotron[28] radiation, mass analysed threshold ionization (MATI)[29] and pulsed field ionization photoelectron (PFI-PE)[30] spectra of the ground ionic state, and electron momentum spectroscopy.[31] Fragmentation studies have also been performed.[32,33] Theoretical predictions for the orbital binding energies[25,26,34] and the valence shell photoelectron spectra[26,34,35] have been obtained.

The HeI excited photoelectron spectra of cis-dichloroethene reveal that some of the outer valence bands exhibit vibrational progressions, although the rather low resolution employed in these studies limits the observable structure. Assignments were proposed through comparison of vibrational energies measured in the ionic states with known molecular ground state values. Such procedures often provide a satisfactory overall interpretation of vibrational structure associated with isolated electronic states, but, as will be shown, more sophisticated methods are required for perturbed states.[12]

II. EXPERIMENTAL APPARATUS AND PROCEDURE

Experimental measurements were made using a VG Scienta R4000 hemispherical electron energy analyser mounted on the soft X-ray undulator-based PLÉIADES beamline at the SOLEIL synchrotron radiation facility, and followed procedures we have previously reported.[36,37] Further details concerning our use of this beamline and endstation are provided as Supplementary Material.

Under the conditions employed here the anticipated optical resolution varied between 0.9 meV at $h\nu = 20$ eV and 5.0 meV at $h\nu = 90$ eV, while the electron

spectrometer resolution was predicted to be 5 meV. Translational Doppler broadening also contributes to the overall observed peak width.[38] Such contributions amount to 4.1 and 11.4 meV for electrons ejected from cis-dichloroethene with kinetic energies of 10.3 or 80.3 eV (corresponding to the formation of the $\tilde{X}\ ^2B_1$ state in the vibrationally unexcited level using photon energies of 20 or 90 eV, respectively).

Dichlorethene is a liquid with a significant vapour pressure at room temperature. The vapour was introduced into the experimental chamber, without heating, after removing dissolved air and volatile impurities.

The normalised photoelectron angular distribution, $I(\theta)$, can be written as

$$I(\theta) = 1 + \beta P_2(\cos\theta),$$

where P_2 is the second Legendre polynomial, and θ the angle between the electron emission and the polarization vector. We extract the anisotropy parameter, β, from spectra recorded with polarizations set perpendicular and parallel to the spectrometer axis, as described in Supplementary Material. Also described there is the method to simulate so-called "magic angle" spectra having relative intensities that are independent of any angular variations (β parameters).

III. COMPUTATIONAL DETAILS

Geometry optimization, and thence vertical ionization energies and vibrational parameters were calculated using standard methods, as noted below and implemented in the Gaussian09 package.[39] Harmonic normal mode analyses for the ground state neutral and ion were obtained using density functional theory (DFT) calculations with the B3LYP functional and cc-pVTZ basis. For the electronically excited ion states, time-dependent (TD-) DFT calculations were

made using the same functional and basis. Franck-Condon simulations of the vibrational structuring of the various photoelectron bands, including Duschinsky rotation of the modes between ground and ion states, were then performed using the FC-Lab II package.[40] To facilitate visual comparison with experiment, the calculated harmonic frequencies were scaled by a factor of 0.97 in accordance with common practice.[41] To provide a more realistic appearance, but not necessarily an exact match to the experimental band profiles, the resulting stick spectra were broadened by convolution to an empirically chosen width of 75 cm^{-1} (~10 meV FWHM).

Calculations of photoionization cross sections and photoelectron anisotropy parameters were made using the CMS-Xα method, following procedures which we have described previously.[11] Here, we adopt the same approach and parameter choices for defining a model potential in which the electron dynamics can be investigated as in recent applications to dichlorobenzene isomers.[19-21] Starting from atomic coordinates derived from a B3LYP/cc-pVTZ geometry optimization, the potential was constructed as overlapping spherical regions situated on the atomic centres in which the exchange contribution to an effective one-electron potential is represented using the Xα local density approximation. Solutions are obtained as expansions in a symmetry adapted basis of spherical harmonic functions: for the neutral ground state these expansions are truncated at l_{max} values of 6 (outer sphere), 4 (non-hydrogenic atoms), and 2 (H atoms); for the continuum electron these values are increased to 18, 12, 9, respectively. We have systematically checked for adequate convergence of the calculated photoionization matrix elements, and hence cross section and anisotropy parameters, against variation of these l_{max} choices. The results presented here are sensitive to neither the choice of equilibrium geometry calculation nor the sphere radii.

IV. RESULTS AND DISCUSSION

Figure 2 shows an overview of the outer valence shell photoelectron spectrum of cis-dichloroethene obtained at a photon energy of 20.5 eV. The calculations reported by Trofimov et al.[12] find that at binding energies below 14.58 eV the single particle model of ionization[42] is adequate; the $\tilde{F}\ ^2A_1$ band may, in contrast, contain contributions from satellite states. Consequently, the lowest six bands, $\tilde{X}$– $\tilde{E}$, will receive most attention in the following discussion.

A. Vibrational analysis of the photoelectron bands

Most of the photoelectron bands due to the outer valence orbitals display vibrational structure. Our calculated vibrational frequencies for the neutral molecule and the $\tilde{X}\ ^2B_1$, $\tilde{A}\ ^2B_2$ and $\widetilde{D}\ ^2B_1$ cation states are listed in Supplementary Material (Tables S-I and S-II). In discussing the vibrational excitations accompanying ionization from the vibrationally unexcited level in the neutral ground state, the vibrational transition is denoted n^k (or for hot bands, n_l^k) where *n* is the number of the vibrational mode, *k* the number of vibrational quanta in final state (and *l* is the vibrational quanta in the initial state – if not 0). The vibrational modes are numbered as recommended by Herzberg.[43] This convention can, however, create some apparent inconsistencies between the mode labelling in the neutral ground state and the cation structures, particularly for the $\widetilde{D}$ state ion. This, we calculate, distorts to a double minimum, non-planar (C_2) equilibrium geometry. In the lowered C_2 point group, vibrational modes that were of a_1 and a_2 symmetry in the C_{2v} neutral molecule descend to *a* symmetry and so are merged in a common, reordered list according to the Herzberg prescription, with an analogous adjustment for the b_1 and b_2 symmetry modes. Should the number *n* consequently designate quite dissimilar vibrations in the initial and final states, when discussing hot band excitations to avoid ambiguity we will explicitly designate the neutral ground state as $\overline{n}_l$, with the subscript *l* indicating the number of vibrational quanta in the initial *neutral* mode $\bar{n}$.

Elsewhere v'' and v^+ are used to label vibrational levels in the neutral and ionic states, respectively.

1. The $\tilde{X}\ ^2B_1$ state

The vibrational analysis of the $(3b_1)^{-1}$ $\tilde{X}\ ^2B_1$ state photoelectron band (Figure 3) appears relatively straightforward and our 0K Franck-Condon simulations are in good agreement with the experimental spectrum. Figure 4 shows an expanded view of the photoelectron peak arising mainly from the adiabatic (0 – 0) transition to the $\tilde{X}\ ^2B_1$ state. Although this peak is fairly symmetric, it displays shoulders on both the low and the high binding energy sides, with a small but distinct additional feature at an energy (9.57 eV) falling clearly below the adiabatic transition energy. It is readily deduced that much of the additional experimental structure in this region can be attributed to hot bands originating from thermally populated, low frequency vibrational levels in the molecular ground state.

A hot band simulation in the 0-0 origin region, calculated using harmonic frequencies as described previously for bromobenzene,[37] is shown in Figure 4. As well as transitions originating from the vibrationless neutral level, transitions originating from the $v_4'' = 1$, $v_5'' = 1$, $v_7'' = 1$, $v_8'' = 1$, $v_{12}'' = 1$, $v_5'' = 2$ and $v_7'' = 2$ levels are included. Transitions from other vibrational levels were ignored because their initial populations were predicted to be negligible. The stick heights (proportional to the photoelectron intensity) are given by the Franck-Condon factor for the specific transition multiplied by the appropriate Boltzmann population at 300 K. These simulations indicate that additional features observed in this origin region arise principally from sequence bands having $\Delta v = 0$, particularly those involving the v_5'' or v_7'' modes.[44]

The Franck-Condon stick spectrum in Figure 4 has been convoluted with a Gaussian function of either 13 or 15 meV (FWHM) to achieve a more realistic

appearance. At this photon energy, 20.5 eV, the theoretically estimated broadening of the photoelectron peak in cis-dichloroethene would be expected to have contributions of 4 meV from the translational Doppler effect, 5 meV from the spectrometer bandpass, and 1 meV from the monochromator bandpass, giving an overall estimated resolution of ~6.5 meV. Under these same experimental conditions we recorded a width of 8.8 meV for the peak due to the $(4p)^{-1}\ ^2P_{3/2}$ state in the photoelectron spectrum of krypton.[37] The 13—15 meV width chosen for the convolution of the stick spectrum exceeds these estimates of the instrumental resolution, which may also suggest that some broadening results from the (unresolved) rotational envelope and possibly also from a rotational Doppler effect.[45]

Significantly, after convolution with these shaping functions the maximum of the resulting composite peak is found to be shifted from the adiabatic origin by 0.7 meV towards higher energy. An adiabatic ionization energy of 9.6578 eV was determined in the MATI experiment.[29] Therefore, we have calibrated our binding energy scale by setting the maximum of the first peak in our measured $\tilde{X}\ ^2B_1$ state photoelectron band to 9.6585 eV. [This calibration has been applied to all spectra presented here.]

The 300K hot band simulation is shown spanning the whole $\tilde{X}\ ^2B_1$ state photoelectron band in Figure 3, where it can be seen to further improve the already good agreement with the experimental spectrum. Guided by the full simulation, the principal structure across the complete $\tilde{X}\ ^2B_1$ photoelectron band can be assigned to six progressions involving the ν_2^+, ν_3^+ and ν_4^+ modes, either alone or in combination with each other, and these are indicated in Figure 5. (Experimental binding energies and assignments are collected and listed in Table S-III, Supplementary Material). We obtain energies of 178, 150 and 100 meV for the ν_2^+, ν_3^+ and ν_4^+ modes, respectively. These values have been

obtained simply as the difference between the binding energy, quoted with an uncertainty of ± 1 meV, of the photoelectron peak due to the 2^1, 3^1 or 4^1 transition, and that of the peak due to the adiabatic transition. All our reported vibrational energies have been estimated in this manner. These values are consistent with those of 177.1, 148.3 and 100.3 meV, respectively, determined in the MATI study.[29] In the neutral ground state, $\tilde{X}$ $^1A_1$, the corresponding vibrational energies are 196.8, 146.2 and 88.2 meV.[44] In addition to the main progressions, our hot band simulations suggest that the feature observed at 9.64 eV can be attributed primarily to transition 7_1^1 with weaker contributions from 5_1^0 and 5_2^1. Similarly, a feature on the opposite side of the adiabatic peak, at 9.681 eV is attributed to a group of close transitions 5_n^{n+1} , where *n* = 0,1,2. A further weak feature at 9.729 eV is ascribed in part to the transition 7^2. Transitions involving the ν_7 mode, which is of a_2 symmetry, were also observed in the MATI experiment.[29] Finally, a predicted transition $7_1^1 4^1$ at 9.74 eV may just be discerned in Figure 5 as a weak shoulder on the side of the second principal peak at 9.76 eV.

2. The $\tilde{A}$ $^2B_2$, $\tilde{B}$ $^2A_1$ and $\tilde{C}$ $^2A_2$ states

Figure 6 shows the $\tilde{A}$ $^2B_2$ state photoelectron band, together with a 0K Franck-Condon simulation. The simulations predict that the vibrational structure arises mainly from three progressions, all involving the ν_5^+ mode, with two of the progressions also involving the excitation of an additional one or two quanta of the ν_4^+ mode. Binding energies of the principal vibrational peaks seen in the experimental spectrum are collected in Table S-IV (Supplementary Material). A vibrational energy of ~27 meV for the ν_5^+ mode can be derived from the experimental spectrum, in good agreement with the calculated value of 26.9 meV (see Table S-I, Supplementary Material).

In preparing Figure 6 the simulated spectrum energy scale has been aligned such that the peak due principally to the 5^{29} excitation coincides with the most intense peak occurring at 11.706 eV in the experimental spectrum. As our simulations place the 5^{29} excitation 0.754 eV above the adiabatic transition, this suggests an adiabatic ionization energy of 10.95 eV. However, this is effectively a long extrapolation back down the ladder of harmonic oscillator levels, and so its reliability may be questioned. In our companion paper[12] we obtain by calculation an alternative estimate of 11.43 eV for the $\tilde{A}\ ^2B_2$ state adiabatic ionization energy.

While the $\tilde{A}\ ^2B_2$ state band (Figure 6) seems to exhibit fairly regular vibrational structure in the low binding energy region up to ~11.76 eV, there is a clear perturbation above this energy that is not seen in the Franck-Condon model. Beyond this, the experimental spectrum starts to merge with the adjacent $\tilde{B}\ ^2A_1$ state band.

Inspection of the complex $\tilde{B}\ ^2A_1$ and $\tilde{C}\ ^2A_2$ state photoelectron bands (Figure 2) shows no recognizable regular vibrational structure in either, and Franck-Condon simulations performed as previously offer no meaningful comparisons. According to our calculations,[12] the binding energy region between 11.2 and 13.0 eV encompasses only the $\tilde{A}\ ^2B_2$, $\tilde{B}\ ^2A_1$ and $\tilde{C}\ ^2A_2$ states and is devoid of satellites. We may thus infer the possibility of vibronic interstate interactions in the region above ~11.76 eV, but the photoelectron anisotropy parameters measured across this binding energy region will provide further insight (vide infra).

The influence of vibronic coupling, which we therefore infer from our experimental results, has been examined theoretically in a companion paper.[12] These calculations predict conical intersections between the potential energy surfaces associated with the $\tilde{A}\ ^2B_2$ and $\tilde{B}\ ^2A_1$ states, and those associated with

the $\tilde{B}$ $^2A_1$ and $\tilde{C}$ $^2A_2$ states, respectively at 11.87 and 12.39 eV. These results go some way to corroborate that the low binding energy region of the $\tilde{A}$ $^2B_2$ state photoelectron band might be interpreted within the adiabatic approximation. In contrast, the bands corresponding to the $\tilde{B}$ $^2A_1$ and $\tilde{C}$ $^2A_2$ states should be strongly affected by non-adiabatic dynamics, and this leads to the observed highly complex vibronic structure.

3. The $\widetilde{D}$ $^2B_1$ and $\tilde{E}$ $^2B_2$ states

The $\widetilde{D}$ $^2B_1$ state photoelectron band shows rather distinct vibrational structure in the low binding energy region but, as seen in Figure 2, merges with the essentially featureless $\tilde{E}$ $^2B_2$ state band to higher energy, losing such definition. Vibronic coupling calculations[12] predict that the $\widetilde{D}$ $^2B_1$ and $\tilde{E}$ $^2B_2$ states lie virtually on top of each other with a very low point of conical intersection. Hence, complicated vibrational profiles might be expected for these two states. Nevertheless, it again appears worthwhile attempting to interpret some of the observed structure using Franck-Condon simulations for the $\widetilde{D}$ $^2B_1$ state. Calculations reveal that the $\widetilde{D}$ $^2B_1$ state cation adopts a twisted non-planar equilibrium geometry (C_2 symmetry); the corresponding harmonic vibrational frequencies appear in Table S-II (Supplementary Material). Both cc-pVDZ and cc-pVTZ basis sets were used for calculations, the former results being used here as providing a very marginally better fit with the experimental spectrum. A 300K hot band spectrum was computed, as for the $\tilde{X}$ band, by the inclusion of transitions originating from the thermal single quantum excitation of v_5'', v_6'', v_7'', v_{11}'', and v_{12}'' and double quanta excitation of v_5'' and v_6''. Transitions from other vibrational levels were ignored because their initial populations were predicted to be negligible. The $\widetilde{D}$ $^2B_1$ band simulation is compared with the experimental spectrum in Figure 7.

The simulations provide a reasonably good description of the overall shape of the observed photoelectron band although some perturbed intensities, and to a lesser extent energy shifts, are evident. An interpretation of the vibrational structure based simply on the measured binding energies suggests that the experimental spectrum can be associated with three progressions. A comparison with the calculated vibrational energies (Table S-II, Supplementary Material) indicates that two of these progressions should be assigned as 5^n and $6^1 5^n$. This results in energies of 46 and 73 meV for the ν_6^+ and ν_5^+ modes, respectively, in good agreement with the B3LYP/cc-pVDZ calculated values of 48.0 and 73.4 meV, respectively. The assignment of the third progression is less certain but the most likely assignment seems to be $6^2 5^n$. The binding energies of the structure belonging to these three progressions are given in Table S-IV (Supplementary Material), where the progressions are labelled P2 – P4. In addition to these three progressions, at energies below that due to the adiabatic transition, peaks occurring at 13.496 and 13.537 eV probably arise as hot band transitions from ν_4" and ν_7" (note that because of the differing electronic state symmetries these neutral molecule vibrational modes are not the same as ν_4^+ and ν_7^+ in the $\widetilde{D}\ ^2B_1$ state ion). An assignment of 7^1 for the small peak observed at 13.610 eV is suggested by the simulation results, despite a small energy mismatch.

The main difference suggested by our simulations to the interpretation given above is the participation of the ν_4^+ mode, which can be categorised as a twisting torsional mode around the C-C axis. Our calculations indicate that the largest contribution to the peak observed at 13.677 eV corresponds to the 4^1 excitation, with the 6^2 excitation playing only a minor role. According to the Franck-Condon predictions, most excitations correspond to combination bands involving the ν_4^+, ν_5^+ and ν_6^+ modes, and these combination bands do not form regular progressions. Adding to the difficulty in assigning the vibrational structure is the fact that the sum of the energies for the ν_4^+ and ν_6^+ modes is almost equal to

twice the energy of the v_5^+ mode (Table S-II, Supplementary Material). It should also be borne in mind, again, that any vibronic coupling between the $\widetilde{D}\ ^2B_1$ and $\tilde{E}\ ^2B_2$ states may modify the vibrational energies considerably.

4. The $\tilde{F}\ ^2A_1$ state

The photoelectron band associated with the $\tilde{F}\ ^2A_1$ state (Figure 8) displays structure which can be assigned to two progressions, each involving a mode with an energy of ~75 meV, with one of the progressions having an additional, single excitation, of a mode with an energy of ~25 meV. The observation of a mode with an energy of 75 meV, a value which is similar to that corresponding to the v_5^+ mode in the $\widetilde{D}\ ^2B_1$ state, suggests that the $\tilde{F}\ ^2A_1$ state cation may also possess C_2 symmetry. Unfortunately, we have been unable to calculate the $\tilde{F}\ ^2A_1$ state geometry and hence determine the energies of the vibrational modes. Therefore, two unassigned progressions, labelled P5 and P6, are shown in Figure 8 and listed in Table S-IV (Supplementary Material).

B. Photoionization dynamics of the outer valence states

Photoelectron anisotropy parameters and branching ratios for the outer valence states are plotted in Figures 9 and 10, respectively. These measurements were made by repeating the recording of the photoelectron spectra, for both horizontal and vertical linear polarization, at selected photon energies across the extended range 19 — 90 eV. The β parameters and branching ratios attributed to each orbital ionization were obtained by integrating over the binding energy regions specified in Table II, with error bars estimated from the Poisson count statistics of the summed count.

The branching ratios (Figure 9) appear to divide into two distinct behaviours, displaying either a minimum or a maximum around 40 eV. Of course, it should be borne in mind that as the branching ratios are normalized to unity, the minima occurring in the branching ratios for the $9b_2$, $10a_1$ and $2a_2$ orbitals will

necessarily give rise to maxima in those of the other orbitals. In general, a very satisfactory agreement is obtained between the experimental and theoretical results shown in Figure 9. (The structure in the calculated ratios below 20 eV can be discounted as largely spurious, due to the staggered threshold values, and the rapidly varying cross sections in this region.) The most significant discrepancy occurs for the branching ratios of the $\widetilde{D}\ ^2B_1$ and $\tilde{E}\ ^2B_2$ states, where the measured branching ratio for the $\widetilde{D}\ ^2B_1$ state is larger than predicted, especially around 40 eV, with that for the $\tilde{E}\ ^2B_2$ state displaying the opposite behaviour. Two factors may account for this discrepancy. The first is associated with the procedure used to analyse the experimental data, where the photoelectron intensity corresponding to a specific state is simply set by the binding energy region (Table II). This procedure makes no allowance for overlapping bands, which is likely to occur for the $\widetilde{D}\ ^2B_1$ and $\tilde{E}\ ^2B_2$ states. The second factor concerns vibronic coupling where the contributions from the individual states are mixed and separation is invalid.

The agreement exhibited between the experimental and calculated β anisotropy parameters (Figure 10) is also very satisfactory. Notably the $\tilde{A}\ ^2B_2$, $\tilde{B}\ ^2A_1$, $\tilde{C}\ ^2A_2$, and $\widetilde{D}\ ^2B_1$ states are predicted to have a pronounced dip at photon energies of 40 — 50 eV (electron kinetic energies of ~30 eV). This dip is due to the Cooper minimum associated with the atomic Cl 3p orbital. Such behaviour is well understood for atomic photoionization, and particularly for p-type orbitals which are relevant to the present study.[17] Electric dipole selection rules restrict the orbital angular momentum of a photoelectron ejected from an initial orbital *l* to *l* ± 1, and theoretical work has shown[15,16] that the radial matrix element for the dominant *l* → *l* + 1 transition (in our case the p → d transition) can change sign provided that the initial wave function contains a node. Thus, at the energy coinciding with the change in sign, the photoionization partial cross section should exhibit a minimum (often referred to as a Cooper minimum). Moreover,

at this energy the photoelectron anisotropy parameter depends solely on the contribution from the l – 1 channel (s-type continuum in our case). For atomic photoionization from a p-orbital, the l – 1 channel possesses an isotropic angular distribution, corresponding to $\beta = 0$. Thus, in the vicinity of the Cooper minimum associated with the Cl 3p orbital, both the anisotropy parameter and the photoionization partial cross section (branching ratio) should exhibit a characteristic and easily recognisable behaviour. The degree to which these atomic properties are observable in the photoionization dynamics of molecular orbitals depends upon the extent to which the molecular orbitals retain their atomic properties.

We now consider the energy dependence of the β anisotropy parameters for the outer valence orbitals in relation to their predicted Mulliken atomic populations (Table I and Figure 1). The experimental β parameter for the outermost $3b_1$ orbital, with the smallest predicted Cl 3p content, shows little evidence of the Cooper minimum. Instead, it exhibits a behaviour typical of that observed[18-21,37,46] and calculated[19-21,37] for a π-type orbital, namely, a rapid rise from a low value at threshold to reach a high plateau value above $h\nu \approx 50$ eV.

The influence of the Cooper minimum is, in contrast, clearly evident in the measured and calculated anisotropy parameters for the $9b_2$, $10a_1$ and $2a_2$ orbitals. Indeed, the deep minimum at a photon energy of ~40 eV is almost as pronounced as that calculated for the atomic Cl 3p orbital.[17] The Mulliken atomic populations for these three orbitals indicate that they may be considered as essentially Cl 3p lone-pairs, and that they retain to a large degree their atomic properties. The next orbital, $2b_1$, has a mixed chlorine and carbon character (Table I). The calculated anisotropy parameter for this orbital shows a reduced dip in the β-value in the region encompassing the Cooper minimum, but also a greater deviation between theory and experiment. As already discussed, this

discrepancy may be due, at least in part, to the data analysis procedure and/or to vibronic coupling. The experimental and calculated β parameters for the $8b_2$ and $9a_1$ orbitals exhibit weak minima in the vicinity of the Cl Cooper minimum, in accord with the predicted small chlorine content of these two orbitals.

Figures 11, 12, and 13 provide examples to show variations in the β parameter measurements derived from the polarization dependent spectra across, respectively, the $\tilde{X}, \widetilde{A}/\tilde{B}$, and $\widetilde{D}/\tilde{E}$ band regions. For the $\tilde{X}$ band recorded at a photon energy of 25 eV (Figure 11) the β parameter remains virtually constant across all the vibrational peaks in the photoelectron spectrum, and this observation is repeated at all other photon energies. This behaviour is consistent with expectations from the Franck-Condon Principle, in which electronic and vibrational motions are considered fully decoupled. Although we do not show examples here, the $\tilde{C}$ $^2A_2$ and $\tilde{F}$ $^2A_1$ states have similarly flat, constant β parameter curves across the respective photoelectron band profiles.

The $\tilde{A}$ $^2B_2$ band anisotropy parameters (Figure 12) behave rather differently. Across the low energy binding region of the band the β parameter remains relatively constant. A shallow increase in β in the $h\nu$ = 31 eV example can in fact be rather trivially attributed to the concomitant fall in electron energy as one steps through vibrational levels at a fixed photon energy; as seen in Figure 10 there is a rapid change in the electronic (vibrationally unresolved) β parameter due to the Cooper minimum at this photon energy, causing β to rise as the kinetic energy falls. Hence, we can safely conclude that again the Franck-Condon prediction of decoupled electronic and vibrational motion is unchallenged in this region.

However, at 11.75 eV binding energy there are rapid changes in the β values. In the examples shown in Figure 12 there occurs a step increase in β in the $h\nu$ = 19

eV recording, while at $h\nu$ = 31 eV a sharp decrease can be observed, but such seemingly discontinuous changes are observed across the photon energy range measured. These step changes coincide with the onset of the perturbed intensities noted in the vibrational analysis of the band (Section IV.A.2). Prompted by this observation, our analysis of the $\tilde{A}\ ^2B_2$ band β parameter photon energy dependence (Figure 10) was repeated, but using a binding energy window with reduced width, spanning just the perturbed region (11.78 — 11.85 eV). This subset is included in the relevant panel of Figure 10. At the lower photon energies used for our study the perturbed region's β parameter now exceeds that determined for the full band, while at the higher photon energies it is less, much as seen at the two specific photon energies appearing in Figure 12.

What is visually striking in Figure 12, and indeed at the other examined photon energies, is that when β diverges in the perturbed binding energy region of the $\tilde{A}\ ^2B_2$ band it adopts the same values as the adjacent two split $\tilde{B}\ ^2A_1$ band peaks around 12 eV binding energy. The earlier theoretical work performed by Haller et al[8] predicted that the photoelectron anisotropy parameter associated with a peak gaining intensity through vibronic coupling should be similar to that of the state to which it is coupled rather than that characterizing the remainder of the photoelectron band. Thus, our experimental evidence strongly suggests that the $\tilde{A}\ ^2B_2$ and $\tilde{B}\ ^2A_1$ states couple vibronically. This inference, based on our experimental spectra, is consistent with our theoretical results[12] which show that the intensity associated with the peak at 11.8 eV is derived from the neighbouring $\tilde{B}\ ^2A_1$ state, to which the $\tilde{A}\ ^2B_2$ state is vibronically coupled, rather than from the $\tilde{A}\ ^2B_2$ state.

The $\widetilde{D}\ ^2B_1$ band β parameters show evidence for a rather different deviation from the expected Franck-Condon behaviour with a clear variation observed

across the photoelectron band profile. There is distinct structuring in the β curve in Figure 13 that correlates with the assigned vibrational peaks in the photoelectron spectrum; similar observations apply across the photon energy range studied. Any interpretation of the variation in the β parameters will be affected by the overlap between the $\widetilde{D}\ ^2B_1$ and $\tilde{E}\ ^2B_2$ state photoelectron bands, and the division at 14.1 eV implied in the regions listed in Table II is purely nominal. Hence some more gradual transition in observed β values between those associated with the $\widetilde{D}\ ^2B_1$ and $\tilde{E}\ ^2B_2$ states is fully expected. However, the irregularities noted in the $\widetilde{D}\ ^2B_1$ state vibrational analysis (Section IV.3) hint at vibronic coupling between these two states.

In Figure 14 we display the β parameters resolved to the first nine principal peaks in the band and assigned to $\widetilde{D}\ ^2B_1$ vibrational modes as indicated in Figure 7. These peaks belong to short progressions in ν_5^+ in combination with the excitation of 0 or 1 quanta of ν_6^+, and to short progressions in ν_6^+ in combination with the excitation of 0 or 1 quanta of ν_5^+. Examining Figure 14 it may be seen that the excitation of successive levels of ν_5^+ (C-Cl stretching) results in a significant shift in the associated β parameter, that exceeds our estimated statistical error bars. In contrast, the excitation of ν_6^+ (skeletal flexing) does not lead to any significant variation in β. It is, however, interesting to note that the 7_1^0 hot band does appear to have β parameters with significantly lower anisotropy than observed for excitations from the vibrationless level of the neutral. Both these ν_5^+ and hot band observations contradict the Franck-Condon expectation of vibrational modes that are fully decoupled from the electronic degrees of freedom, but from foregoing comments it is clear that a full account of the vibronic coupling needs to be invoked for better understanding of the $\widetilde{D}\ ^2B_1 - \tilde{E}\ ^2B_2$ state photoionization dynamics.

V. CONCLUSIONS

Plane polarized synchrotron radiation has been used to measure photoelectron spectra encompassing the outer valence electronic states of cis-dichloroethene, allowing for analysis of vibrational structure, photoelectron angular distributions, and electronic state branching ratios. The adiabatic approximation appears to be valid for the $\tilde{X}\ ^2B_1$ state, and the vibrational structure observed in the experimental spectrum has been interpreted successfully using Franck-Condon simulations. Similar vibrational analyses have been attempted for the low energy portions of the $\tilde{A}\ ^2B_2$ and $\widetilde{D}\ ^2B_1$ state bands, although perturbations and intensity irregularities are noted, providing a first hint of vibronic interactions with adjacent states.

Using two polarization orientations at multiple selected photon energies across the 19—90 eV range, the energy dependence of photoelectron anisotropy parameters and branching ratios has been determined. The β parameters associated with the $9b_2$, $10a_1$, $2a_2$ and $2b_1$ orbitals, all of which possess a significant Cl 3p character, exhibit an energy dependence reminiscent of that expected for atomic chlorine. Specifically, the β parameters and branching ratios pass through a minimum, at a photon energy of ~40 eV, associated with the Cooper minimum, in good agreement with theoretical calculations for this molecule. Dips in the electronic branching ratio of the $\tilde{A}\ ^2B_2$, $\tilde{B}\ ^2A_1$, $\tilde{C}\ ^2A_2$ states, again attributable to the Cooper minimum, also agree well with theoretical predictions. However, the expected dip in the $\widetilde{D}\ ^2B_1$ state branching ratio is not observed. Neither the $\widetilde{D}\ ^2B_1$ nor the $\tilde{E}\ ^2B_2$ state branching ratio agrees well with adiabatic calculations, further hinting at $\widetilde{D} - \tilde{E}$ state vibronic interactions.

Perhaps the most interesting experimental finding is that the photoelectron anisotropy parameter associated with a peak occurring at a binding energy of 11.8 eV displays the same photon energy dependence as that for the $\tilde{B}\ ^2A_1$ state,

rather than that for the low energy portion of the $\tilde{A}\ ^2B_2$ state, from which we can now infer a strong possibility of vibronic coupling[8] between the $\tilde{A}\ ^2B_2$ and $\tilde{B}\ ^2A_1$ states.

Although of a slightly different character, the photoelectron anisotropy measurements made in the low binding energy region of the $\widetilde{D}\ ^2B_1$ state band also provide evidence of vibronic interaction. Both these observations of vibrational level dependent β values and the perturbations noted in the photoelectron spectrum reveal a breakdown of the adiabatic Franck-Condon approximation for this state.

As is evident from the comparison between our experimental results, Franck-Condon simulations of vibrational structure, and calculated anisotropy parameters and branching ratios, a full account of the vibronic coupling in cis-dichloroethene is required to address the discrepancies between our measured spectra and theoretical predictions. The theoretical modelling of these vibronic interactions is the subject of our companion paper.[12]

ACKNOWLEDGMENTS

A.B.T. & A.D.S. gratefully acknowledge the grant, Grant No. 4.1671.2017/4.6, from the Ministry of Education and Science of the Russian Federation. D.M.P.H. is grateful to the Science and Technology Facilities Council (United Kingdom) for financial support.

We acknowledge the provision of beamtime by Synchrotron Soleil (beamtime Proposal No. 20131329) and we thank the technical staff at Soleil for their support and for the smooth operation of the facility.

We are grateful for access to the University of Nottingham High Performance Computing Facility in support of the computational effort.

References

1 H. Köppel, W. Domcke, and L. S. Cederbaum, Adv. Chem. Phys. **57**, 59 (1984).

2 H. Köppel, L. S. Cederbaum, W. Domcke, and S. S. Shaik, Angewandte Chemie-International Edition in English **22**, 210 (1983).

3 H. Köppel, W. Domcke, L. S. Cederbaum, and W. von Niessen, J. Chem. Phys. **69**, 4252 (1978).

4 H. Köppel, L. S. Cederbaum, and W. Domcke, J. Chem. Phys. **77**, 2014 (1982).

5 A. Hazra and M. Nooijen, Phys. Chem. Chem. Phys. **7**, 1759 (2005).

6 A. Hazra and M. Nooijen, J. Chem. Phys. **122** (2005).

7 D. M. P. Holland, D. A. Shaw, M. A. Hayes, L. G. Shpinkova, E. E. Rennie, L. Karlsson, P. Baltzer, and B. Wannberg, Chem. Phys. **219**, 91 (1997).

8 E. Haller, H. Köppel, L. S. Cederbaum, G. Bieri, and W. von Niessen, Chem. Phys. Lett. **85**, 12 (1982).

9 E. Haller, H. Köppel, L. S. Cederbaum, W. von Niessen, and G. Bieri, J. Chem. Phys. **78**, 1359 (1983).

10 D. M. P. Holland, M. A. MacDonald, M. A. Hayes, L. Karlsson, and B. Wannberg, Chem. Phys. **226**, 351 (1998).

11 Y. Hikosaka, J. H. D. Eland, T. M. Watson, and I. Powis, J. Chem. Phys. **115**, 4593 (2001).

12 A. B. Trofimov, I. Powis, R. C. Menzies, D. M. P. Holland, E. Antonsson, M. Patanen, C. Nicolas, C. Miron, A. D. Skitnevskaya, E. V. Gromov, and H. Köppel, J. Chem. Phys. Accepted : ED Number A18.04.0046

13 R. S. Mulliken, J. Chem. Phys. **23**, 1833 (1955).

14 D. W. Turner, C. Baker, A. D. Baker, and C. R. Brundle, *Molecular photoelectron spectroscopy : a handbook of He 584 A spectra*. (Wiley-Interscience, London, 1970).

15 J. W. Cooper, Phys. Rev. **128**, 681 (1962).

16 U. Fano and J. W. Cooper, Reviews of Modern Physics **40**, 441 (1968).

17 S. T. Manson, A. Msezane, A. F. Starace, and S. Shahabi, Phys. Rev. A **20**, 1005 (1979).

18 A. B. Trofimov, J. Schirmer, D. M. P. Holland, L. Karlsson, R. Maripuu, K. Siegbahn, and A. W. Potts, Chem. Phys. **263**, 167 (2001).

19 A. W. Potts, D. M. P. Holland, I. Powis, L. Karlsson, A. B. Trofimov, and I. L. Bodzuk, Chem. Phys. **415**, 84 (2013).

20 I. Powis, A. B. Trofimov, I. L. Bodzuk, D. M. P. Holland, A. W. Potts, and L. Karlsson, Chem. Phys. **415**, 291 (2013).

21 D. M. P. Holland, I. Powis, A. B. Trofimov, I. L. Bodzuk, D. Y. Soshnikov, A. W. Potts, and L. Karlsson, Chem. Phys. **448**, 61 (2015).

22 N. Jonathan, K. Ross, and V. Tomlinson, Int. J. Mass Spec. Ion Phys. **4**, 51 (1970).

[23] R. F. Lake and H. Thompson, Proceedings of the Royal Society of London Series a-Mathematical and Physical Sciences **315**, 323 (1970).

[24] K. Wittel and H. Bock, Chem. Ber.-Recl. **107**, 317 (1974).

[25] K. Kimura, S. Katsumata, Y. Achiba, T. Yamazaki, and S. Iwata, *Handbook of HeI Photoelectron Spectra of Fundamental Organic Compounds*. (Japan Scientific Societies Press, Tokyo, 1981).

[26] W. von Niessen, L. Åsbrink, and G. Bieri, J. Elec. Spec. Rel. Phen. **26**, 173 (1982).

[27] A. Berndtsson, E. Basilier, U. Gelius, J. Hedman, M. Klasson, R. Nilsson, C. Nordling, and S. Svensson, Phys. Scrip. **12**, 235 (1975).

[28] J. F. Ying and K. T. Leung, J. Elec. Spec. Rel. Phen. **63**, 75 (1993).

[29] Y. J. Bae and M. S. Kim, Int. J. Mass. Spec. **267**, 89 (2007).

[30] K. C. Lau, H. K. Woo, P. Wang, X. Xing, and C. Y. Ng, J. Chem. Phys. **124**, 224311 (2006).

[31] L. Mei, M. Chuaqui, C. P. Mathers, J. F. Ying, and K. T. Leung, J. Chem. Phys. **101**, 3558 (1994).

[32] M. A. Parkes, S. Ali, C. R. Howle, R. P. Tuckett, and A. E. R. Malins, Mol. Phys. **105**, 907 (2007).

[33] A. Bodi, W. R. Stevens, and T. Baer, J. Phys. Chem. A **115**, 726 (2011).

[34] V. Galasso, Theochem-J. Mol. Struct. **337**, 249 (1995).

[35] K. Takeshita, J. Chem. Phys. **110**, 6792 (1999).

[36] J. Soderstrom, A. Lindblad, A. N. Grum-Grzhimailo, O. Travnikova, C. Nicolas, S. Svensson, and C. Miron, New J. Phys. **13**, 073014 (2011).

[37] I. Powis, D. M. P. Holland, E. Antonsson, M. Patanen, C. Nicolas, C. Miron, M. Schneider, D. Y. Soshnikov, A. Dreuw, and A. B. Trofimov, J. Chem. Phys. **143**, 144304 (2015).

[38] P. Baltzer, L. Karlsson, M. Lundqvist, and B. Wannberg, Rev. Sci. Inst. **64**, 2179 (1993).

[39] M. J. Frisch, G. W. Trucks, H. B. Schlegel, G. E. Scuseria, M. A. Robb, J. R. Cheeseman, G. Scalmani, V. Barone, B. Mennucci, G. A. Petersson, H. Nakatsuji, M. Caricato, X. Li, H. P. Hratchian, A. F. Izmaylov, J. Bloino, G. Zheng, J. L. Sonnenberg, M. Hada, M. Ehara, K. Toyota, R. Fukuda, J. Hasegawa, M. Ishida, T. Nakajima, Y. Honda, O. Kitao, H. Nakai, T. Vreven, J. J. A. Montgomery, J. E. Peralta, F. Ogliaro, M. Bearpark, J. J. Heyd, E. Brothers, K. N. Kudin, V. N. Staroverov, T. Keith, R. Kobayashi, J. Normand, K. Raghavachari, A. Rendell, J. C. Burant, S. S. Iyengar, J. Tomasi, M. Cossi, N. Rega, J. M. Millam, M. Klene, J. E. Knox, J. B. Cross, V. Bakken, C. Adamo, J. Jaramillo, R. Gomperts, R. E. Stratmann, O. Yazyev, A. J. Austin, R. Cammi, C. Pomelli, J. W. Ochterski, R. L. Martin, K. Morokuma, V. G. Zakrzewski, G. A. Voth, P. Salvador, J. J. Dannenberg, S. Dapprich, A. D. Daniels, O. Farkas, J. B. Foresman, J. V. Ortiz, J. Cioslowski, and D. J. Fox, Gaussian 09 Revision D.01 (Gaussian Inc., Wallingford, CT, 2013).

[40] I. Pugliesi and K. Muller-Dethlefs, J. Phys. Chem. A **110**, 4657 (2006).

[41] J. P. Merrick, D. Moran, and L. Radom, J. Phys. Chem. A **111**, 11683 (2007).

[42] L. S. Cederbaum, W. Domcke, J. Schirmer, and W. Von Niessen, Adv. Chem. Phys. **65**, 115 (1986).

[43] G. Herzberg, *Molecular spectra and molecular structure II. Infared and raman spectroscopy*. (D. Van Nostrand, 1945).

[44] T. Shimanouchi, *Tables of Molecular Vibrational Frequencies Consolidated Volume 1*. (NBS, 1972).

[45] Y. P. Sun, C. K. Wang, and F. Gel'mukhanov, Phys. Rev. A **82** (2010).

[46] D. M. P. Holland, L. Karlsson, and W. von Niessen, J. Elec. Spec. Rel. Phen. **113**, 221 (2001).

Tables

Table I. Mulliken atomic population in the outer valence molecular orbitals of cis-dichloroethene (units are electrons; sum over all atoms is 2) calculated at the HF/cc-pVTZ level.[12]

Atom	$3b_1$ (π)	$9b_2$ ($\sigma_{Cl\ LP}$)	$10a_1$ ($\sigma_{Cl\ LP}$)	$2a_2$ ($\pi_{Cl\ LP}$)	$2b_1$ ($\pi_{Cl\ LP}$)	$8b_2$ (σ)	$9a_1$ (σ)	$8a_1$ (σ)
C	0.58	0.04	0.08	0.06	0.40	0.33	0.39	0.59
H	0.01	0.02	0.05	0.0	0.0	0.15	0.0	0.28
Cl	0.41	0.94	0.87	0.94	0.59	0.52	0.61	0.13

Table II. Energy regions used in the analysis of the photoelectron spectra recorded with plane polarized synchrotron radiation.

Orbital	Binding energy region (eV)
$3b_1(\pi)$	9.5 – 10.8
$9b_2(\sigma_{Cl\ LP})$	11.2 – 11.9
$10a_1(\sigma_{Cl\ LP})$	11.9 – 12.3
$2a_2(\pi_{Cl\ LP})$	12.3 – 13.1
$2b_1(\pi_{Cl\ LP})$	13.4 – 14.1
$8b_2(\sigma)$	14.1 – 15.0
$9a_1(\sigma)$	15.3 – 16.2

Figure captions

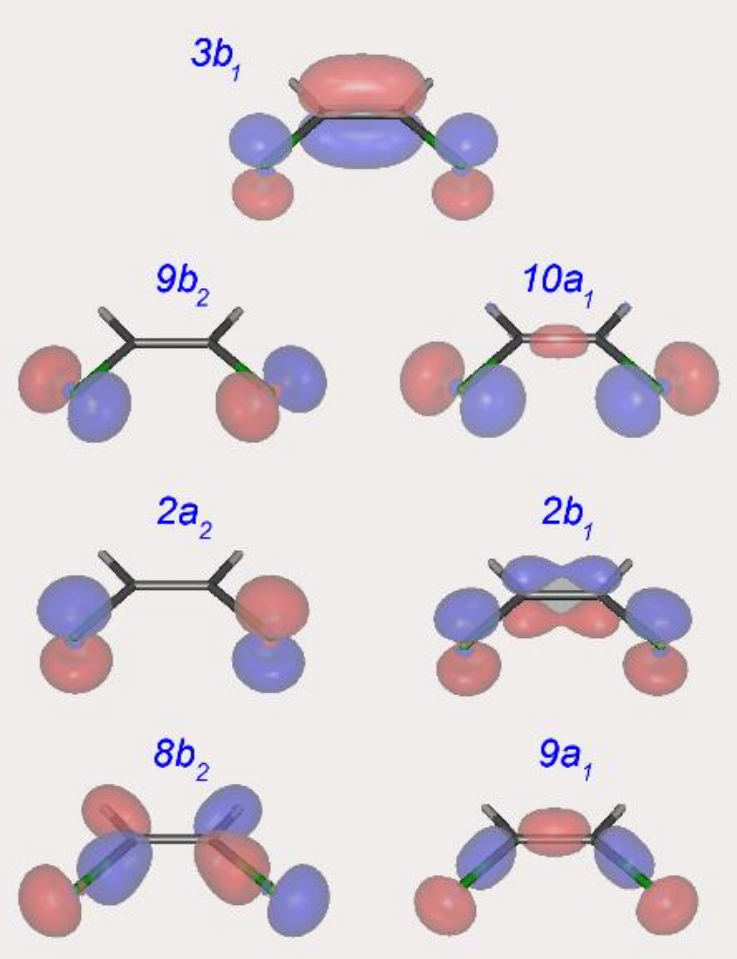

Figure 1.

The outer valence orbitals of cis-dichloroethene.

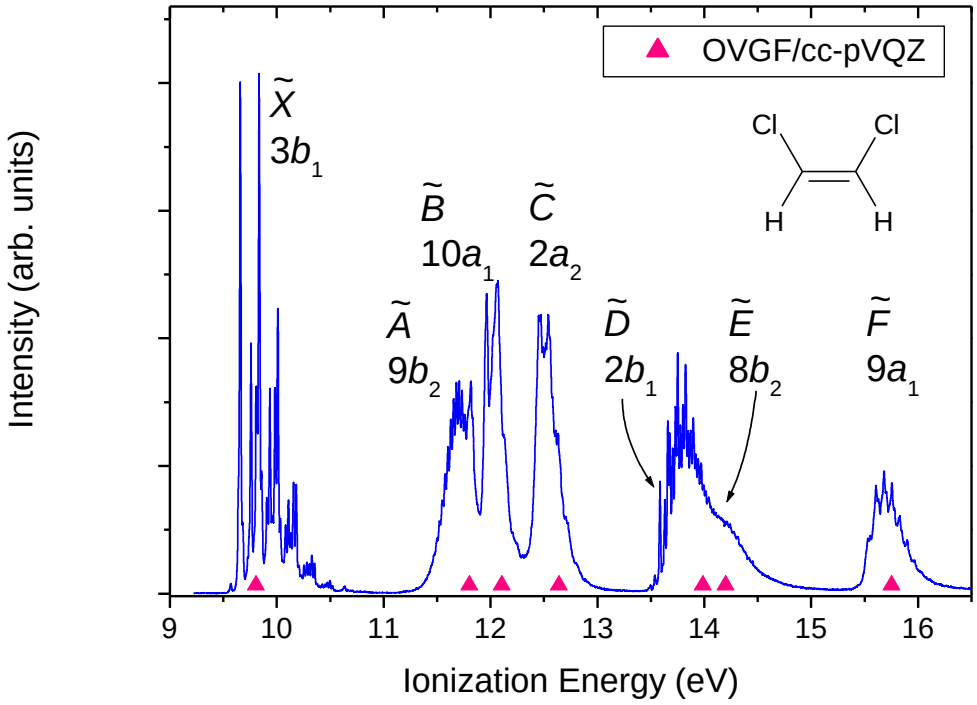

Figure 2

The outer valence shell photoelectron spectrum of cis-dichloroethene recorded at a photon energy of 20.5 eV. States are labelled as being due to ionization from a single molecular orbital. Also marked along the bottom axis are calculated OVGF/cc-pVQZ vertical ionization energies.

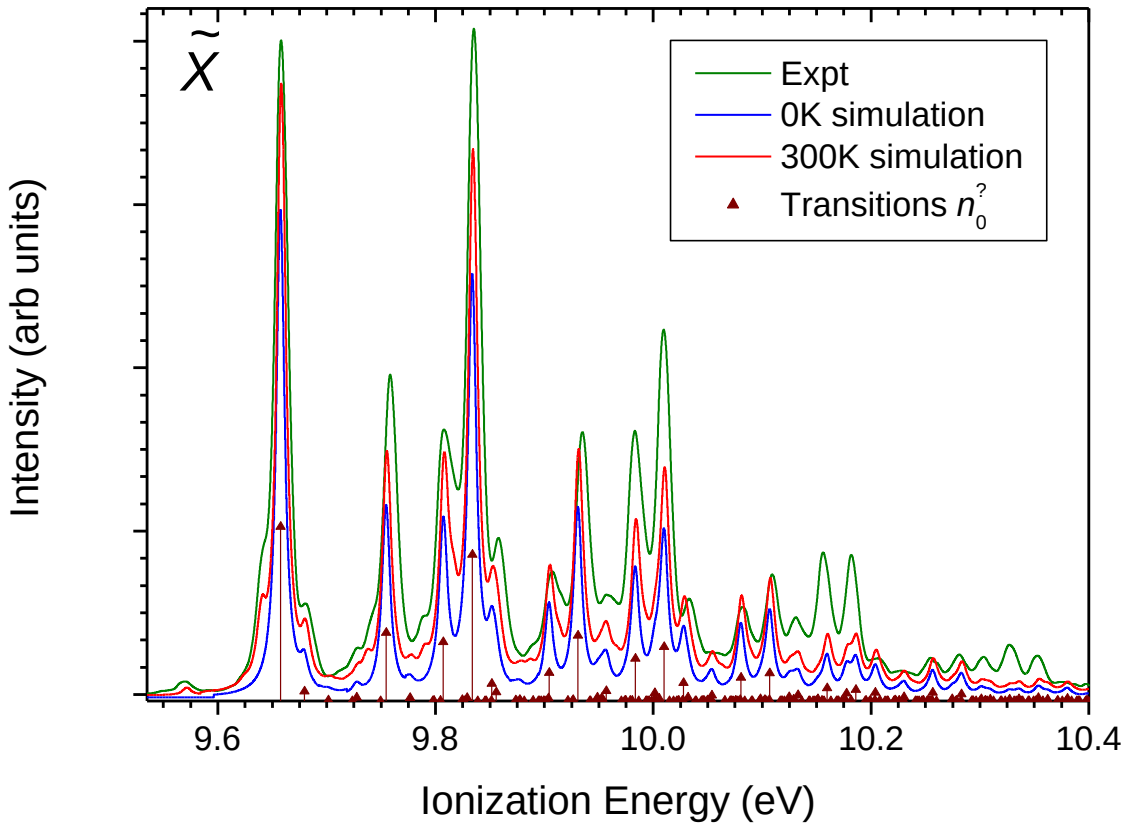

Figure 3

Experimental $\tilde{X}\ ^2B_1$ state photoelectron band of cis-dichloroethene (recorded with $h\nu$=20.5 eV) and a cold (0K) Franck-Condon simulation using B3LYP/cc-pVTZ calculated vibrational modes, with harmonic frequencies scaled by a factor of 0.985. The calculated stick spectrum is convoluted with a shaping function to provide more realistic visual comparison. Also shown is a second simulated spectrum that includes hot bands arising from an assumed 300K thermal population of the lower frequency neutral ground state modes.

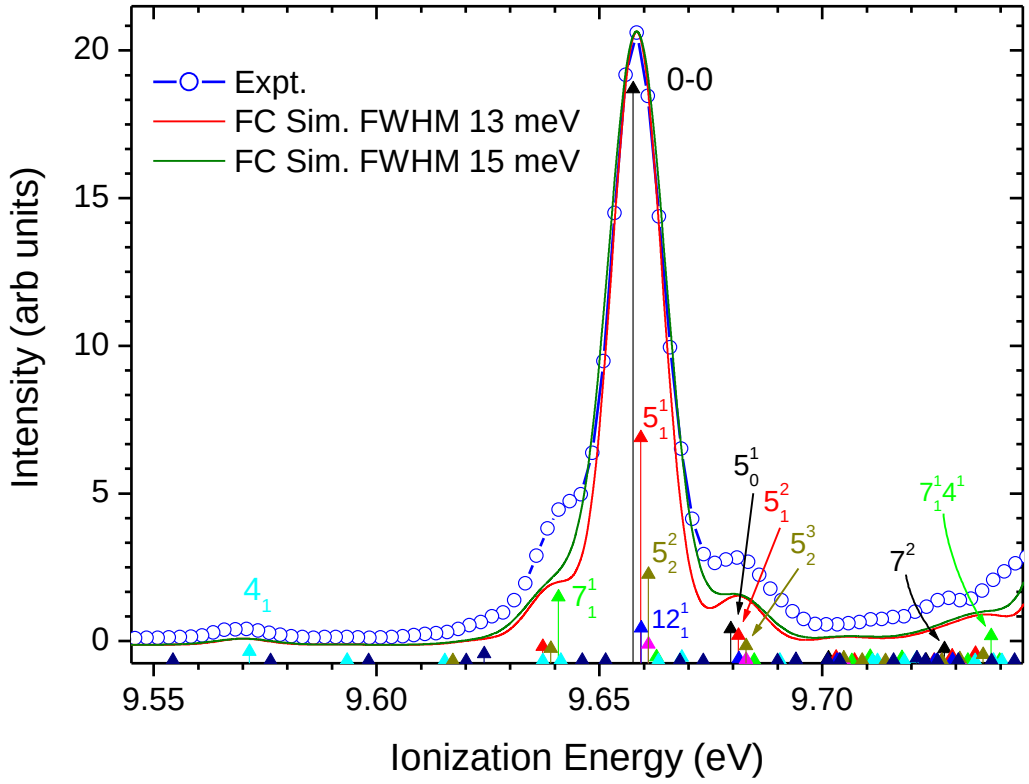

Figure 4

Expanded vibrational origin region of the $\tilde{X}\ ^2B_1$ photoelectron band of cis-dichloroethene (Figure 2) comparing the experimental spectrum (recorded with $h\nu$=20.5 eV) and B3LYP/cc-pVTZ Franck-Condon simulations. The latter are shown both as a stick spectrum, and convoluted with Gaussian functions having either 13 meV or 15 meV FWHM for more realistic comparisons. The stick spectrum is colour coded to indicate those transitions having a common lower level, and the assignments for the most prominent peaks (similarly colour coded) are included in the figure. For clarity small vertical offsets are applied between the curves showing experimental and simulated spectra.

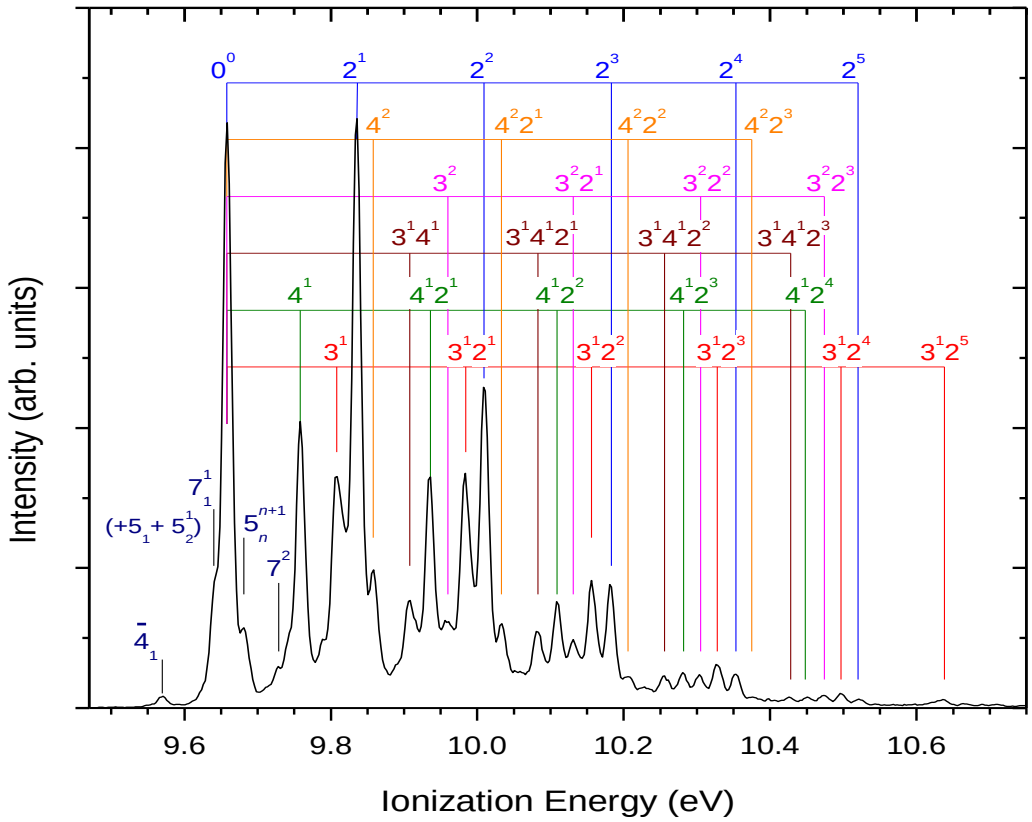

Figure 5

The cis-dichloroethene $\tilde{X}\ ^2B_1$ photoelectron band with vibrational assignments of transitions from the vibrationless neutral ground state shown. Some identified hot band assignments are also shown (see Figure 4).

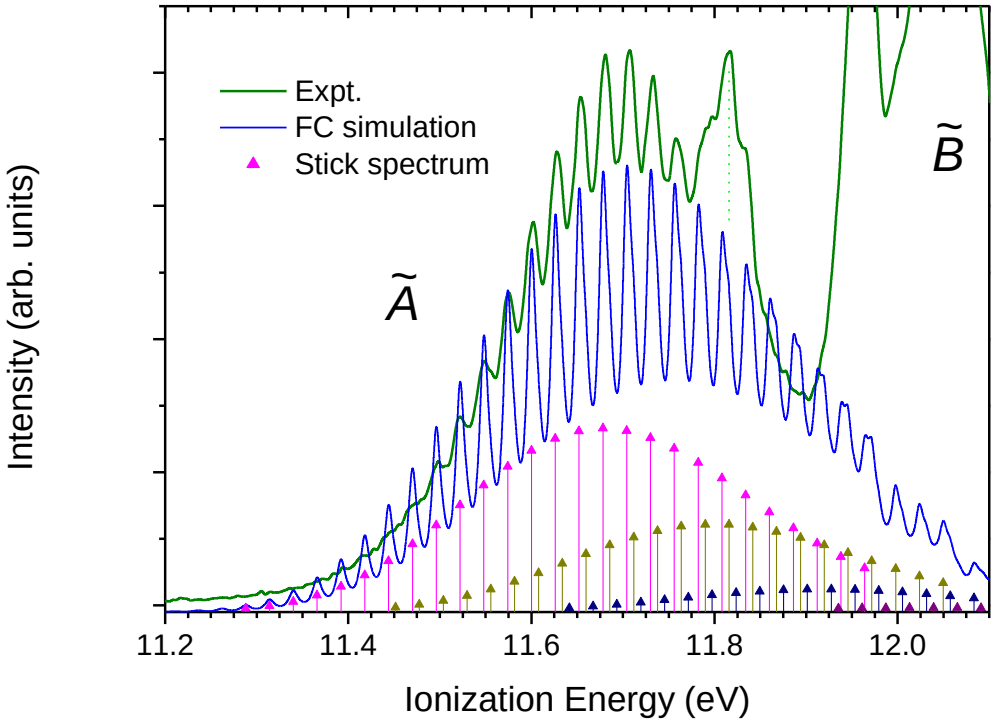

Figure 6

Experimental photoelectron spectrum of cis-dichloroethene in the $\tilde{A}\ ^2B_2$ band region, (recorded with $h\nu$ = 20.5 eV) and a cold (0K) Franck-Condon simulation using B3LYP/cc-pVTZ calculated vibrational modes, with harmonic frequencies scaled by a factor of 0.968. The principal structure is identified as three long progressions in the ν_5^+ mode, building on zero (magenta), one (olive), or two (navy) quanta of the ν_4^+ mode. The calculated stick spectrum is convoluted with a shaping function to provide more realistic visual comparison.

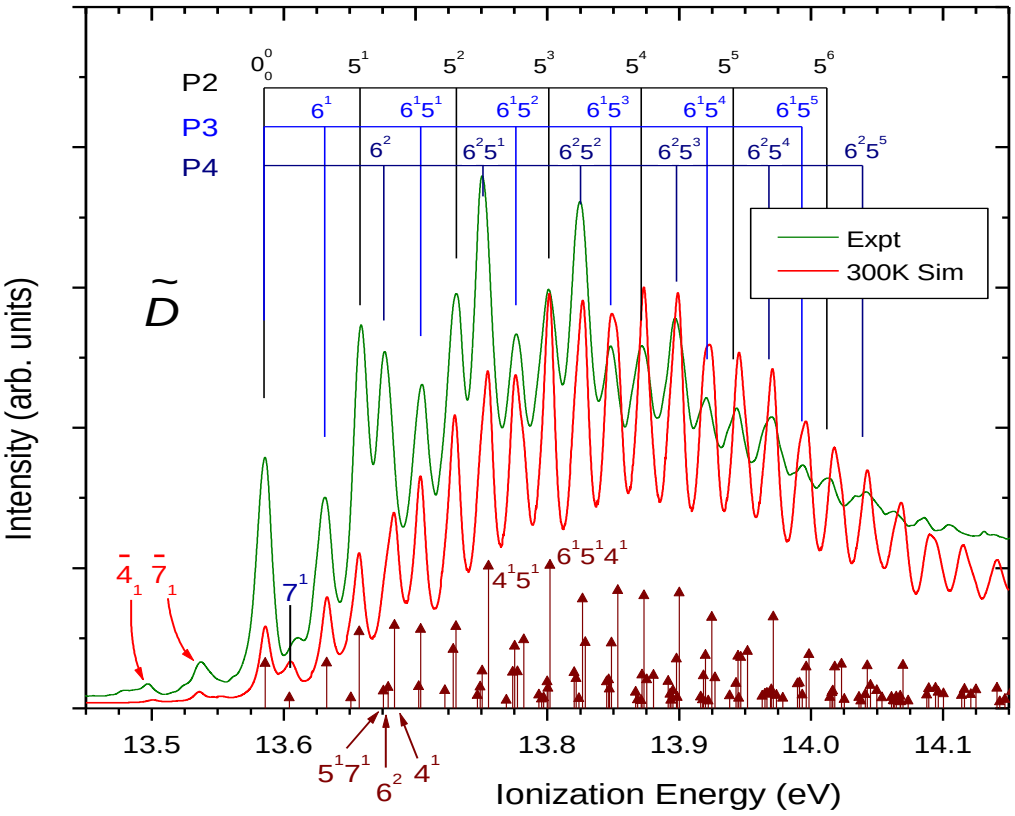

Figure 7

Experimental photoelectron spectrum of cis-dichloroethene in the $\tilde{D}\ ^2B_1$ band region (recorded with $h\nu$ = 20.5 eV) and a Franck-Condon simulation using calculated B3LYP/cc-pVDZ harmonic frequencies, scaled by a factor 0.972. The convoluted stick spectrum (curve) includes calculated 300K hot bands, but for clarity only the positions of transitions from the vibrationless ground state are marked. Three progressions, P2 — P4, determined from the experiment are indicated and are listed in Supplementary Material, Table S-IV.

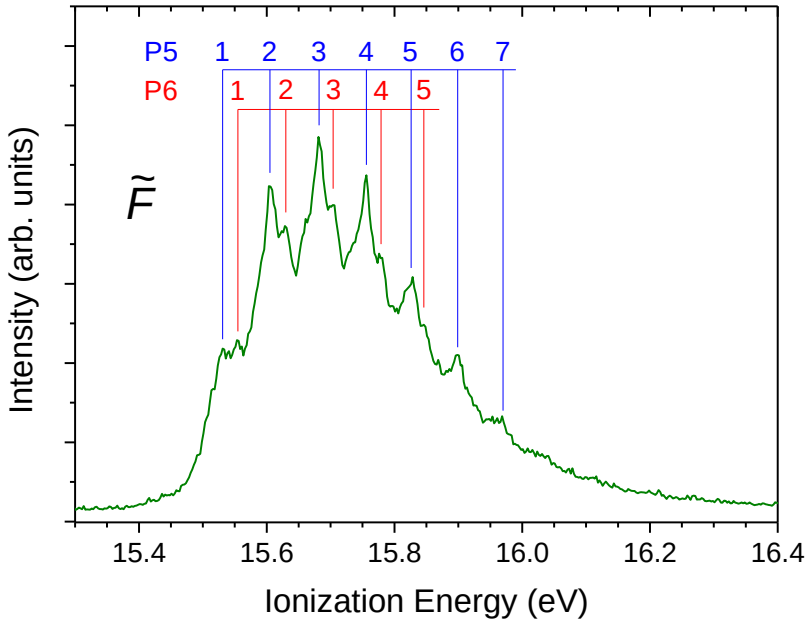

Figure 8

Experimental $\tilde{F}\ ^2A_1$ photoelectron band (recorded with hν = 20.5 eV) with two identified progressions, P5 and P6.

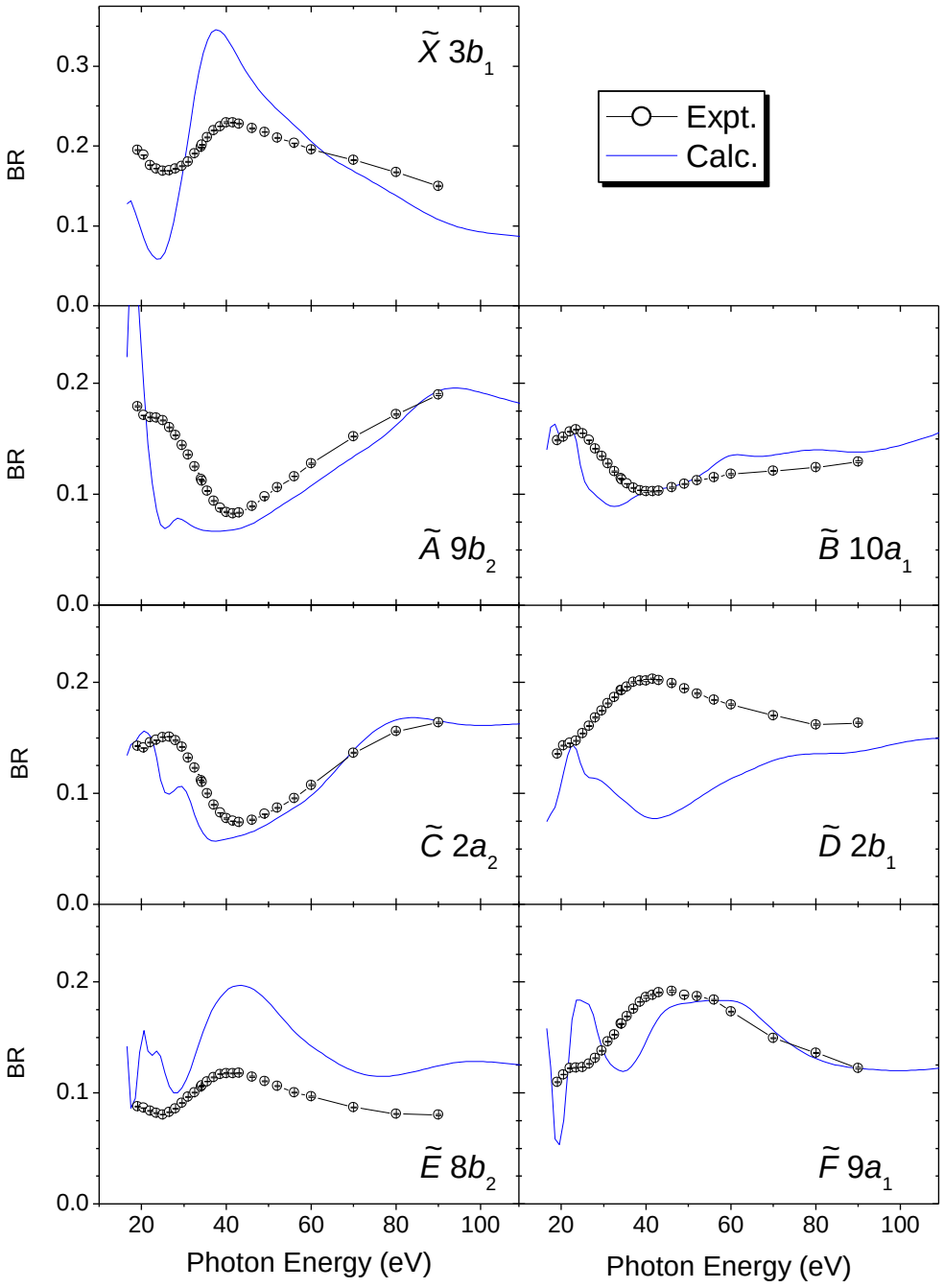

Figure 9

Experimental and theoretical (CMS–Xα) outer valence electronic state branching ratios for cis-dichloroethene. Experimental data are sampled over the binding energy ranges specified in Table II. Error bars representing the statistical uncertainty only are plotted but are usually smaller than the plotting symbol.

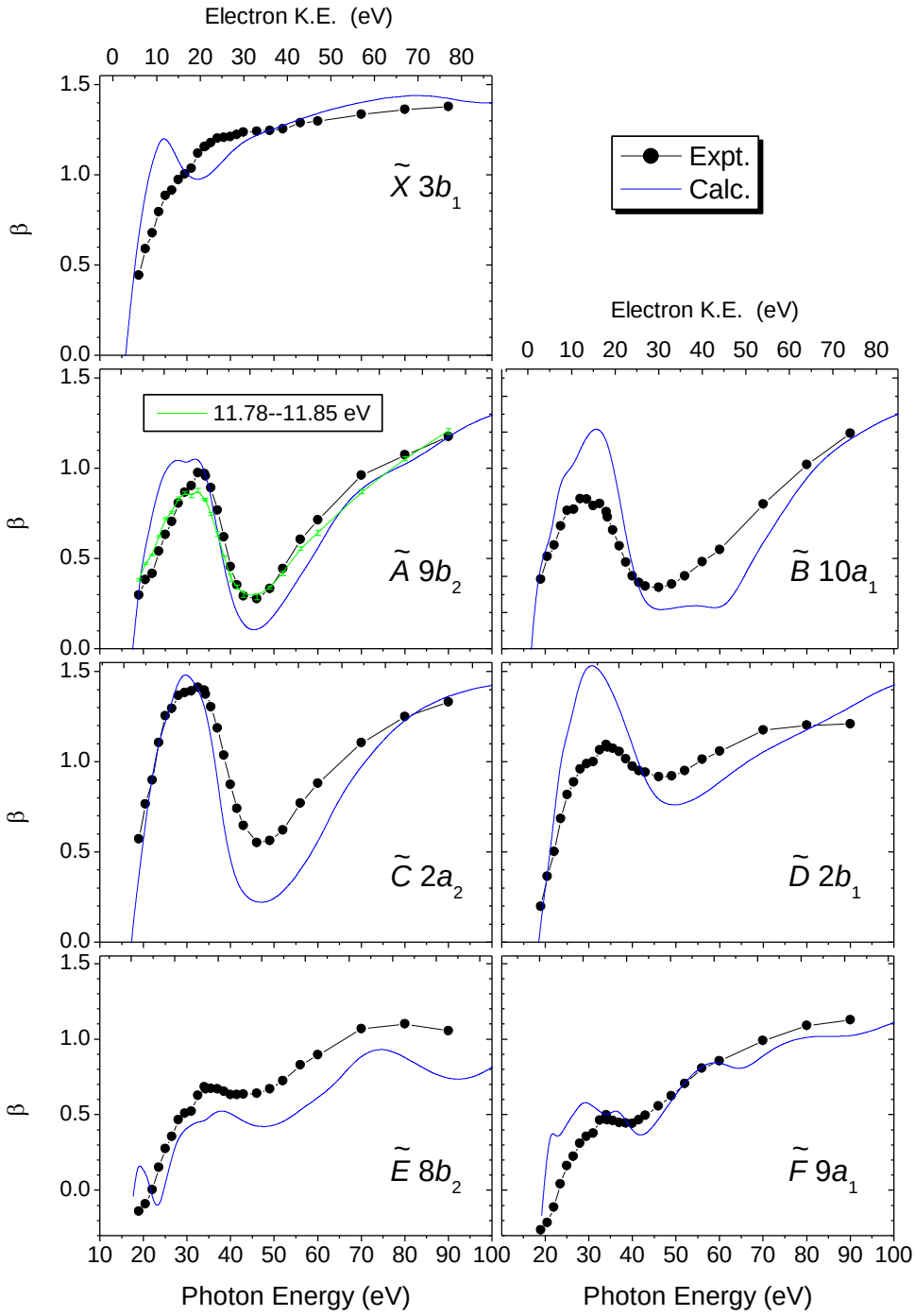

Figure 10

Experimental and calculated photoelectron anisotropy parameters, β, for the outer valence states of cis-dichloroethene. Experimental data are sampled over the binding energy ranges specified in Table II, while the $\tilde{A}\ ^2B_2$ state band data

includes a supplementary analysis made on a reduced size window region, 11.78 eV — 11.85 eV. Error bars on the experimental results represent the statistical uncertainty only, but usually are smaller than the plotting symbol. The CMS-Xα calculations are plotted with an offset of +3 eV to compensate the overestimated attraction of the Xα potential.

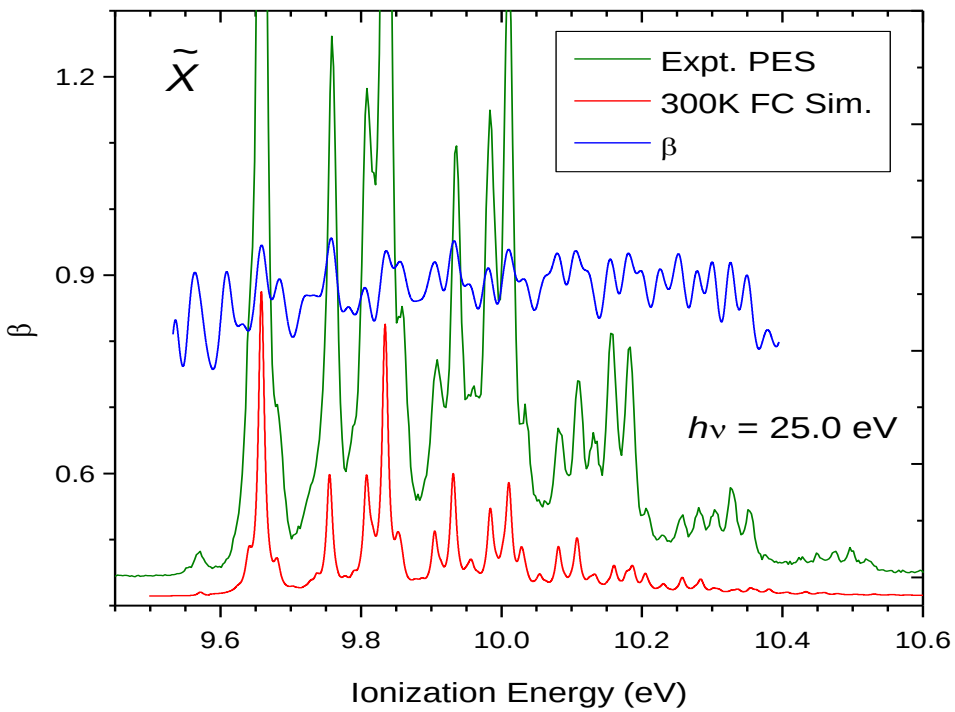

Figure 11.

β parameter measurement across the $\tilde{X}\ ^2B_1$ photoelectron band, recorded with 25 eV photon energy. The experimental "magic angle" photoelectron spectrum (PES) is plotted on the same energy scale for direct comparison with the measured β. Also included for comparison is the 300K Franck-Condon simulation. Both the experimental and simulated spectra are arbitrarily scaled. The former uses an expanded vertical scaling for clarity, with the result that the most intense peaks are clipped (see Figure 3)

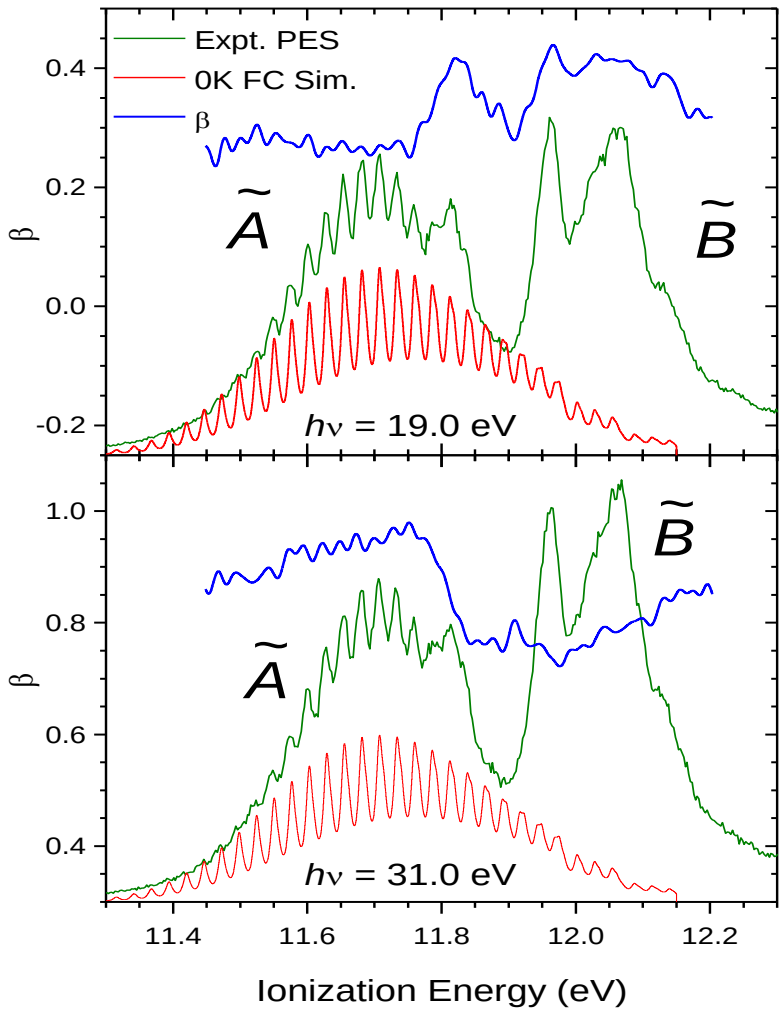

Figure 12

Examples of the β parameter measurements across the $\tilde{A}/\tilde{B}$ band region of the photoelectron spectrum, recorded at two different photon energies: 19 eV (top) and 31 eV (bottom). For direct comparison the corresponding "magic angle" photoelectron spectra (PES) are plotted on the same energy scale. Also included for reference is the 0K Franck-Condon simulation. Both experimental and simulated photoelectron spectra are arbitrarily scaled.

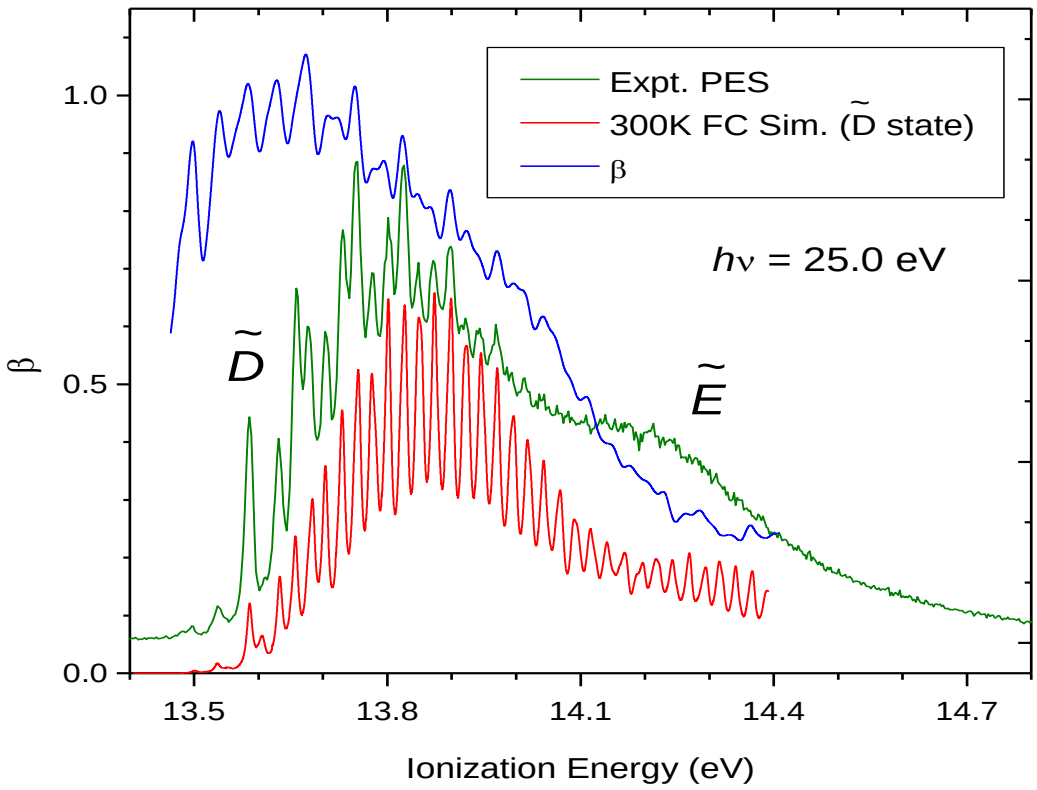

Figure 13

β parameter measurement across the $\tilde{D}/\tilde{E}$ band region of the photoelectron spectrum, recorded with 25 eV photon energy. The experimental "magic angle" photoelectron spectrum (PES) is plotted on the same energy scale for direct comparison with the measured β. Also included for reference is the 300K Franck-Condon simulation. Both the experimental and simulated spectra are arbitrarily scaled.

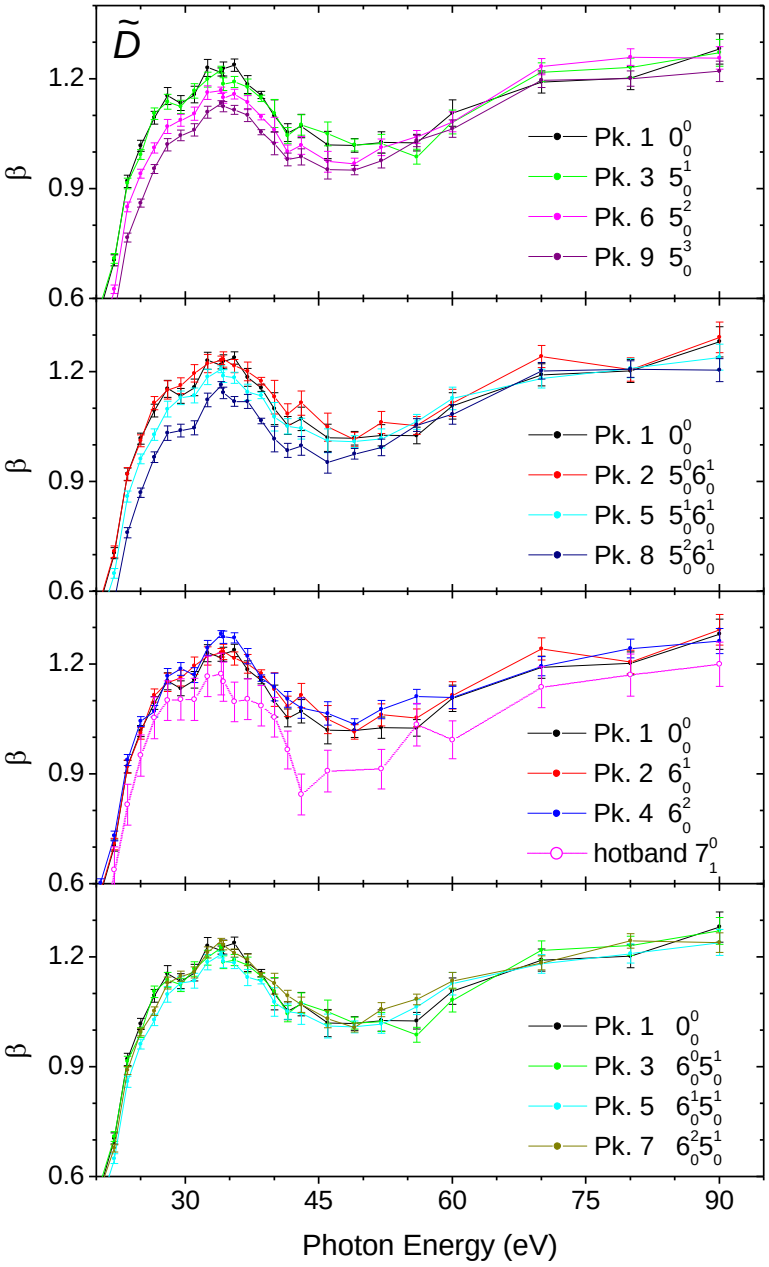

Figure 14

Vibrationally resolved $\widetilde{D}$ $^2B_1$ state β parameters, labelled according to assignments in Figure 7. For clarity these measurements are separately displayed as progressions in: ν_5^+in combination with 0 or 1 quanta in ν_6^+ (upper panels); ν_6^+ in combination with 0 or 1 quanta in ν_5^+ (lower panels). Alongside the pure progression in ν_6^+ the anisotropy of the hot band $\overline{7}_1^0$ is also shown. Error bars are estimated from the Poisson counting statistics.